BIOCHEMISTRY
including biophysical chemistry & molecular biology

Article

pubs.acs.org/biochemistry

Luminescence Resonance Energy Transfer in the Cytoplasm of Live *Escherichia coli* Cells

Daniel González,[†] Nayanish Lokhande,[†] Swaraj Vadde,[†] Qi Zhao,[†] Aaron Cassill,[†] and Robert Renthal*[,†,‡]

[†]Department of Biology, University of Texas at San Antonio, San Antonio, Texas 78249, United States

[‡]Department of Biochemistry, University of Texas Health Science Center at San Antonio, San Antonio, Texas 78229, United States

ABSTRACT: Luminescence resonance energy transfer (LRET) offers many advantages for accurate measurements of distances between specific sites in living cells, but progress in developing a methodology for implementing this technique has been limited. We report here the design, expression, and characterization of a test protein for development of a LRET methodology. The protein, which we call DAL, contains the following domains (from the N-terminus): *Escherichia coli* dihydrofolate reductase (DHFR), the third and fourth ankyrin repeats of $p16^{INK4a}$, a lanthanide-binding tag (LBT), and a hexahistidine tag. LBT binds Tb^{3+} with a submicromolar dissociation constant. LRET was measured from the Tb^{3+} site on LBT to transition metals bound to the hexa-His tag and to fluorescein methotrexate bound to DHFR. The measured distances were consistent with a molecular model constructed from the known crystal structures of the constituent domains of DAL. The results indicate that the two C-terminal ankyrin domains of $p16^{INK4a}$ are stably folded when combined with other protein domains. We found that Tb^{3+} binds to DAL in the cytoplasm of live *E. coli* cells, and thus, DAL is useful as an indicator for studies of metal transport. We also used DAL to measure LRET from Tb^{3+} to Cu^{2+} in the cytoplasm of live *E. coli* cells. The rates of Tb^{3+} and Cu^{2+} transport were not affected by a proton uncoupler or an ATP synthase inhibitor. Reversal of the membrane potential had a small inhibitory effect, and removal of lipopolysaccharide had a small accelerating effect on transport. Changing the external pH from 7 to 5 strongly inhibited the Tb^{3+} signal, suggesting that the Tb^{3+}–LBT interaction is useful as a cytoplasmic pH indicator in the range of approximately pH 5–6.

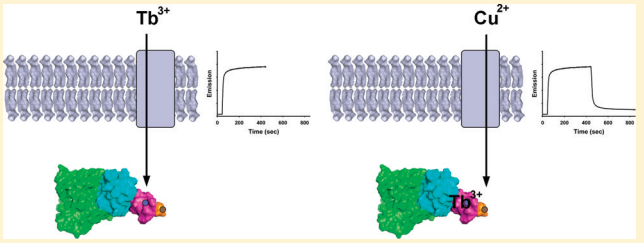

Luminescence resonance energy transfer (LRET) offers advantages over fluorescence-based Förster resonance energy transfer (FRET) for measuring distances between sites on biological macromolecules.[1] The advantages include insensitivity to light scattering or background fluorescence artifacts, less uncertainty about the dipole orientation factor, and the ease of selectively measuring energy donor–acceptor distances without having all donors paired with acceptors. Nevertheless, LRET measurements are not yet widely used. One drawback to the application of LRET is the large expense and lack of availability of lanthanide chelators. This problem has been at least partly solved by the development of genetically encoded LRET donor sites known as lanthanide-binding tags (LBTs).[2−4] The small size of LBTs (~2 kDa molecular mass, ~15 Å diameter) also can provide distance measurements in live cells at a precision higher than that with cnidarian fluorescent proteins (GFP has a 26.8 kDa molecular mass and an ~30 × 40 Å size). LBTs on the extracellular surface of the plasma membrane have been used in live cell measurements,[5] but a fuller exploitation of the LBT's potential will require methods of controlled delivery of lanthanide ions into the cytoplasm. Coordinated lanthanides are not taken up[6] or are mostly delivered to endosomes and lysosomes.[7,8] It is not clear why some chelates target other cytoplasmic compartments.[7,9] We designed a test protein, which we call DAL (dihyrofolate reductase-ankyrin-LBT), to assist the development of lanthanide transfer agents that would be useful in cytoplasmic loading of LBTs. To our surprise, we found that *Escherichia coli* BL21(λDE3) cells freely take up Tb^{3+} at concentrations useful for LRET but not toxic to the cells. We report here on the preparation and characterization of DAL and an application to measure the rates of metal ion transport in *E. coli*.

MATERIALS AND METHODS

Plasmid Construction. The DNA encoding the two C-terminal ankyrin domains of $p16^{INK4a}$[10] was fused to the DNA encoding an LBT domain derived from peptide 1 from Nitz et al.[3] This was generated as a synthetic construct following the method of Stemmer,[11] with the thermophilic nucleases replaced with KOD polymerase (Toyobo, New York, NY), which generates a blunt end product from the following 14 40-mer oligonucleotides: U1ALBT, GGGGCTCAGCGGGCGGCGAACCGAACTGCGCGGATCCGG; U2ALBT, CGACCCTGACCCGCCCGGTGCATGATGCGGCGCGCGAAGG; U3ALBT, CTTTCTGGATACCCTGGTGGTGCTGCATCGCGCGGGCGCG; U4ALBT, CGCCTGGATGTGCGCGATGCGTGGGGCCGCCTGCCGGTGG; U5ALBT, ATCTGGCGGAAGAACTGGGCCATCGCGATGTGGCGCGCTA; U6ALBT, TCTGCGCG-

Received: May 19, 2011
Revised: July 7, 2011
Published: July 8, 2011

CGGCGGCGGGCGGCGGCTATATTGATACCAAC; U7ALBT, AACGATGGCTGGTATGAAGGCGATGAACTG-CTGGCGTAAG; L1ALBT, CCCTCTAGAGGTACCGAATT-CTTACGCCAGCAGTTCATCG; L2ALBT, CCTTCATACCA-GCCATCGTTGTTGGTATCAATATAGCCGC; L3ALBT, CGCCCGCCGCCGCGCGCAGATAGCGCGCCACATCGCG-ATG; L4ALBT, GCCCAGTTCTTCCGCCAGATCCACC-GGCAGGCGGCCCCAC; L5ALBT, GCATCGCGCACATCC-AGGCGCGCGCCCGCGCGATGCAGCA; L6ALBT, CCA-CCAGGGTATCCAGAAAGCCTTCGCGCGCCGCATCATG; L7ALBT, CACCGGGCGGGTCAGGGTCGCCGGATCC GCGCAGTTCGGT.

The resulting blunt end polymerase chain reaction (PCR) product was cloned into the pCR-Blunt cloning vector (Invitrogen, Carlsbad, CA), transformed into the TOP10 strain of *E. coli* (Invitrogen), and confirmed by DNA sequencing. The *E. coli* dihydrofolate reductase gene (DHFR) was obtained from the control plasmid in the PURExpress in vitro protein synthesis kit (NEB, Ipswich, MA). The following primers were used for amplifying DHFR and ankyrin-LBT1 in PCRs using KOD polymerase: UpLeftDHFR, GGAGATATACATATGATCAGT-CTGATTGCGGCGTTAGCGGTAGATCGCGT; Lo-LeftDHFR, TAGGGTGCGGCCTTCAATCCGCCGCTC-CAGAATCTCAAA; UpRightDHFR, TTTGAGATTCTGGAG-CGGCGGATTGAAGGCCGCACCCTA; LoRightDHFR, GTGCTCGAGTGCGGCCGCCAGCAGTTCATCGCC.

The two PCR products were gel purified, and the left and right flanks were fused by using the UpLeftDHFR and LoRightDHFR primers to generate an expected ~780 bp fragment forming the eDHFR−ANK-LBT1 fusion product that was cloned into pCR-Blunt. To express the protein with a hexahistidine affinity tag at the C-terminus, 5′ *Nde*I and 3′ *Xho*I restriction sites were used to ligate the sequence into a pET-21a(+) expression vector (Novagen, Gibbstown, NJ). The cycle 3 GFP mutant of Crameri et al.[12] was modified by mutating Ser 65 to Thr, and the coding sequences for GFP^{S65T} were inserted into the pET-21a(+) vector containing the ankyrin-LBT1 sequences to produce what we call GAL, a GFP^{S65T}-ANK-LBT1-hexa-His tag construct.

Protein Expression and Purification. The pET-21 vector containing the coding sequence for DAL was used to transform *E. coli* strain BL21(λDE3). The cells were induced with 1% α-lactose for 17 h at 37 °C, and the cell pellet was extracted with 8 M guanidinium chloride and 1 M Tris (pH 8.0). The extract was diluted 4-fold with water and applied to a Ni-NTA spin column (Qiagen, Valencia, CA). The DAL protein was eluted with imidazole. EDTA was added to the eluate to a concentration of 10 mM, and DAL was then purified on a Superdex 75 column in 10 mM HEPES (pH 7.0) containing 0.1 M NaCl. The protein concentration of the DAL fractions was measured by UV absorbance at 280 nm, using an extinction coefficient of 4.66×10^4 M^{-1} cm^{-1}, derived by combining the measured extinction coefficient for DHFR[13] and the calculated extinction coefficient for the ankyrin and LBT domains (http://www.expasy.ch/tools/protparam.html). Purified DAL was typically obtained at a concentration in the range of 1−4 μM (overall yield of >10 mg/L) . Cells transformed with the pET-21 vector containing the GAL (GFP^{S65T}-ANK-LBT1) construct were induced by methods similar to those described above, expressing the GAL protein, which differs from DAL in that it has GFP^{S65T} instead of DHFR. GAL was purified by the same methods that were used for DAL.

Luminescence Spectroscopy. Emission spectra were measured in a 4 mm path length cuvette on a Photon Technology International, Inc. (Birmingham, NJ) Quantamaster 4 fluorometer using excitation slits with 1 nm bandwidth and emission slits with 5 nm bandwidth. Emission lifetimes were obtained with a Xenoflash phosphorescence accessory operating at 100 Hz, with a 100 μs integration time, using slits with 10 nm bandwidth. Fluorescein methotrexate (FlMTX) was obtained from Biotium (Hayward, CA) and dissolved in dimethylformamide. Spectra were recorded at 23 ± 1 °C.

Modeling. For comparison of LRET results, a model of DAL was constructed from the atomic coordinates of the component domains. We used the following Protein Data Bank (PDB) entries: for DHFR, chain A of 3DRC; for the two ankyrin repeats, residues 67−134 of 1BI7 (tumor suppressor $p16^{INK4a}$); for LBT, 1TJB; and for the hexa-His tag, residues 161−165 of 3PRU. We modeled a starting position for the interaction between DHFR and the ankyrin domain using VMD[14] and then uploaded the coordinates to the RosettaDock server (rosettadock.graylab.jhu.edu/). Of the 10 lowest-energy models produced, we selected the one with the shortest distance between the N-terminus of the ankyrin domain and the C-terminus of DHFR (7.6 Å). We then used VMD to position the LBT domain close to the C-terminus of the ankyrin domain. The position of FlMTX was modeled with the fluorescein-modified cysteine from PDB entry 1DZH. We used Autodock[15] to find a low-energy fluorescein binding site on the liganded DHFR structure (PDB entry 1DRE). Of the 10 lowest-energy models (calculated free energies of binding ranging from −6 to −8 kcal/mol), only one model had the fluorescein in a position that could join with bound methotrexate via a covalent bond.

Metal Transport. Overnight cultures of DAL pET-21 BL21(λDE3) cells were induced for 4 h with 1% α-lactose. Control cells (Top10, Invitrogen) contained a vector derived from pBAD18 that lacked coding sequences for DAL. Cells were washed twice in 10 mM HEPES (pH 7.0) and 0.1 M NaCl and resuspended in that buffer at a cell density of 0.3 mg of dry weight/mL.[16] Some samples were treated with EDTA, following the method of Joshi et al.[17] Samples (2.5 mL) were placed in a 1 cm path length cuvette in the holder of the Quantamaster 4 spectrofluorometer. Cells were gently stirred using a small stirring bar and the built-in stirring motor of the fluorometer. Emission at 545 nm from 280 nm excitation was continuously monitored. Additives were introduced into the stirred cells as follows, with the final concentrations given and the volumes added and stock solution concentrations indicated in parentheses: Tb^{3+}, 50 μM (25 μL, 50 mM $TbCl_3$); Cu^{2+}, 10 μM (2.5 μL, 10 mM $CuSO_4$); dithiothreitol, 2 mM (5 μL, 1 M); glucose, 10 mM (25 μL, 1 M); carbonyl cyanide *m*-chlorophenyl hydrazone (CCCP), 1 μM (2.5 μL, 1 mM in ethanol); dicyclohexylcarbodiimide (DCCD), 50 μM (1.25 μL, 1 M in ethanol); valinomycin, 30 μM (7.5 μL, 10 mM in dimethyl sulfoxide); Ca^{2+}, 1 mM (25 μL, 0.1 M $CaCl_2$). Periplasm was extracted by the method described by Nossal and Heppel.[18]

RESULTS

DAL, a model LBT Protein with LRET Acceptor Sites. The model protein has three domains: *E. coli* dihydrofolate reductase (DHR) at the N-terminus, two ankyrin repeats in the middle, and a lanthanide-binding tag (LBT) with a hexa-His tag at the C-terminus (Figure 1). Hence, we refer to this protein as DAL (dihyrofolate reductase-ankyrin-LBT). DAL

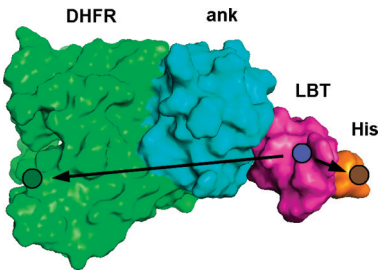

Figure 1. Molecular model of DAL: green for dihydrofolate reductase (DHFR), cyan for ankyrin repeats 3 and 4 from $P16^{INK4a}$, magenta for the lanthanide-binding tag (LBT), and orange for the hexa-His tag. Circles indicate approximate locations of the Tb^{3+} binding site in LBT, the transition metal binding sites in the hexa-His tag, and the fluorescein binding site in DHFR. Arrows indicate approximate donor–acceptor distances. Solvent-accessible surface generated from modeled atomic coordinates using PyMOL Molecular Graphics System, version 1.3 (Schrödinger, LLC).

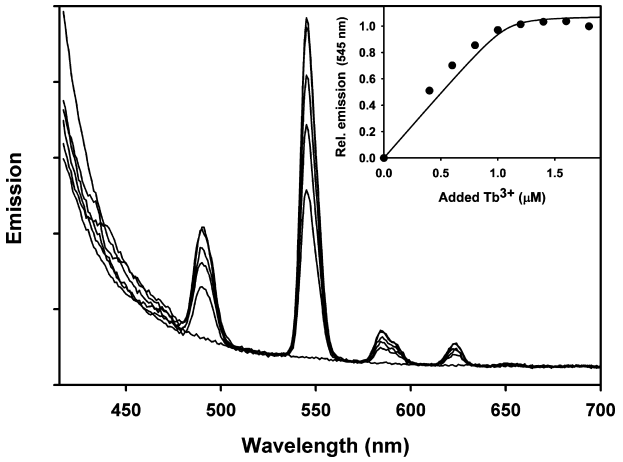

Figure 2. Tb^{3+} binding to DAL. Emission spectra (280 nm excitation) were recorded for DAL (1.1 μM) in 10 mM HEPES buffer (pH 7.0) and 0.1 M NaCl before (bottom curve) and after additions of $TbCl_3$ to final concentrations of 0.4, 0.6, 0.8, 1.2, and 1.4 μM (top curve). All scans were taken at the same instrument settings. The inset shows the Tb^{3+} binding titration. Areas of the 545 nm emission peaks in the spectra, relative to fully bound DAL, are plotted against the amount of added $TbCl_3$. The line was calculated assuming a 10 nM Tb^{3+} dissociation constant.

contains a luminescence donor site on the LBT and two different types of acceptor sites. The hexa-His tag strongly binds transition metals, which act as short-distance energy acceptors for terbium. The Förster critical distances reported for LRET from terbium to transition metals are 12 Å for Ni^{2+} and 20 Å for Cu^{2+}.[5] DHFR strongly binds fluorescein methotrexate (FlMTX),[19] which is a long-distance energy acceptor for terbium. The LRET critical distance reported for the Tb^{3+}–fluorescein complex is 45 Å.[5] We wanted the model protein to have a Tb^{3+}–fluorescein transfer efficiency of ~50%, but the most straightforward attachment sites for LBT (the N- and C-termini of DHFR) are ~30 Å from the FlMTX site. Thus, we inserted two ankyrin repeats as spacers between DHFR and LBT. DAL can be used as a standard for measuring binding of Tb^{3+} to LBT, as well as for short-range LRET to transition metals, and long-range energy transfer to fluorescein.

Tb^{3+} Binding. DAL was titrated with small amounts of added Tb^{3+}, and luminescence emission spectra were recorded (Figure 2). The results are consistent with previously reported Tb^{3+}–LBT dissociation constants.[2−4] After the Tb^{3+} site of LBT was fully bound, the lifetime was measured as 2.12 ms (Figure 3 and Table 1).

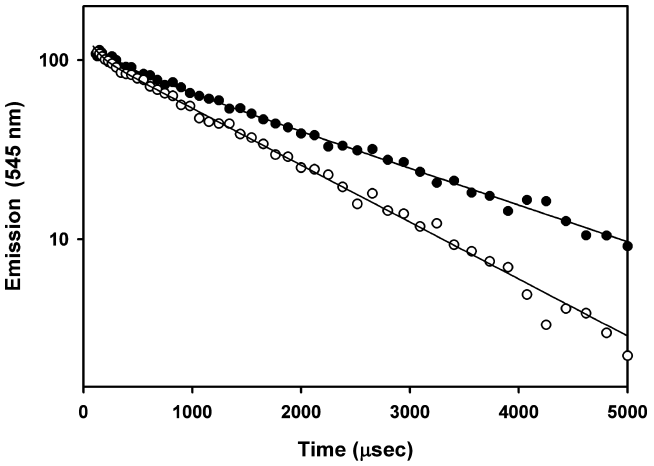

Figure 3. LRET between LBT and the hexa-His tag. DAL (1.1 μM) in 10 mM HEPES (pH 7.0), 0.1 M NaCl, and 1.6 μM Tb^{3+}. Lifetimes measured in the absence (●) and presence (○) of 80 μM $NiCl_2$. Lines fit with lifetimes of 2.12 (●) and 1.37 ms (○). Excitation wavelength of 280 nm.

Table 1. Distance Measurements by Luminescence Resonance Energy Transfer

protein	acceptor	quantum yield ratio (Q_{DA}/Q_D)	lifetime (ms)	transfer efficiency, E	donor–acceptor distance, R (Å)
DAL	Ni^{2+}	0.40		0.60	11
	none		2.12		
	Ni^{2+}		1.37	0.36	13
	Cu^{2+}	0.06		0.94	13
	none		1.99		
	Cu^{2+}		0.35	0.82	15
	FlMTX	0.435		0.56	43
	none		2.05		
	FlMTX		1.04	0.50	45
GAL	GFP		0.62	0.69	43

Transition Metal LRET Acceptors. The Tb^{3+}–DAL complex was titrated with $NiCl_2$, and the emission spectrum was measured after each addition. The Tb^{3+} emission was quenched by Ni^{2+}, as expected for binding to the hexa-His tag that is in the proximity of the LBT. A plot of the areas of the 545 nm Tb^{3+} emission band as a function of Ni^{2+} concentration (Figure 4) indicated that the dissociation constant for dissociation of Ni^{2+} from the DAL hexa-His tag was 8.6 μM. The limiting quenching of Tb^{3+} emission by Ni^{2+} was 0.40, or an energy transfer efficiency of 0.60. This implies that the distance between the Tb^{3+} and Ni^{2+} sites is 11.2 Å (Table 1). Emission decay measurements of DAL with both the Tb^{3+} and Ni^{2+} sites fully occupied (Figure 3) gave a lifetime of 1.37 ms. This indicates a transfer efficiency of 0.36 and a distance of 13.2 Å. The larger amount of quenching measured in the steady state (Figure 4) is likely due to a contribution from exchange interaction,[20] because of the proximity of the two sites. Cu^{2+} was also bound to the DAL hexa-His tag. The

dx.doi.org/10.1021/bi200779u | Biochemistry 2011, 50, 6789–6796

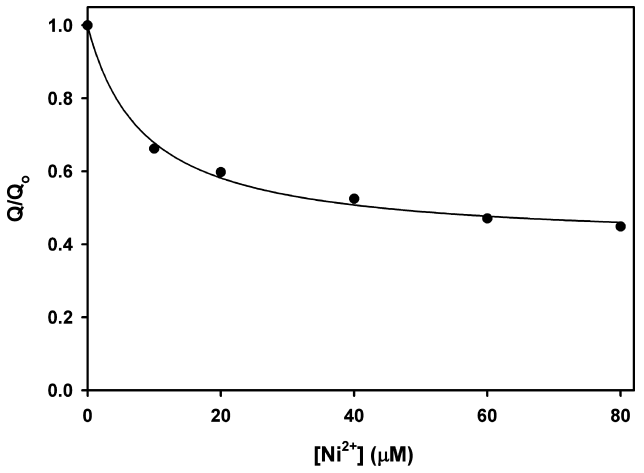

Figure 4. Ni^{2+} binding to DAL. Areas of the Tb^{3+} emission peak at 545 nm from the Tb^{3+}−DAL complex were measured as a function of added Ni^{2+} concentration and plotted as Q/Q_o, the ratio to emission without Ni^{2+}. The line was fitted assuming a single Ni^{2+} binding site on the DAL hexa-His tag with a dissociation constant of 8.6 μM. Same conditions as in Figure 3.

dissociation constant was estimated to be 0.2 μM; the distances measured between Tb^{3+} and Cu^{2+} were 12.6 Å (steady state) and 15.5 Å (lifetime) (Table 1).

Fluorescein LRET Acceptor. The Tb^{3+}−DAL complex was titrated with fluorescein methotrexate (FlMTX), and the emission spectrum was measured after each addition (Figure 5).

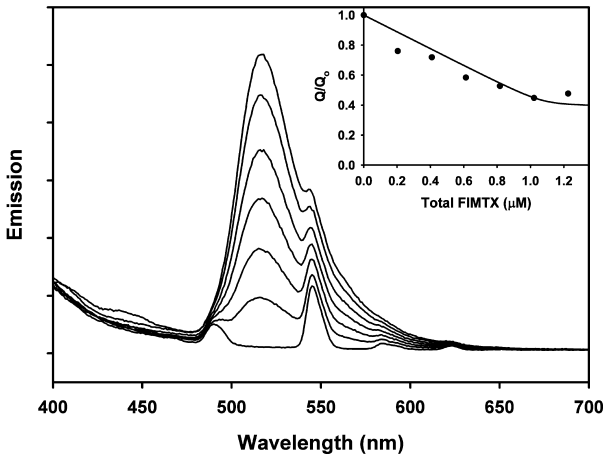

Figure 5. FlMTX binding to DAL. The Tb−DAL complex (1.1 μM) was titrated with FlMTX (0−1.2 μM in increments of 0.2 μM). The excitation wavelength was 280 nm. All scans were taken at the same instrument settings. The inset shows the areas of 545 nm Tb emission peaks plotted as Q/Q_o (ratio to emission without FlMTX) vs total FlMTX. The line was fit with a binding constant of 5 nM.

The Tb^{3+} emission was quenched, as expected for binding of FlMTX to the DHFR domain of DAL. The areas of the Tb^{3+} emission bands at 545 nm were measured (using a baseline extrapolation from the fluorescein emission at wavelengths above and below the Tb^{3+} emission). The results are plotted in the inset of Figure 5 versus the total Tb^{3+} concentration and compared with a line calculated using an FlMTX dissociation constant of 5 nM. The Tb^{3+} emission decay was measured after all the FlMTX sites were filled, monitoring the sensitized emission from fluorescein at 520 nm (Figure 6). The LRET transfer efficiency was calculated from the change in quantum

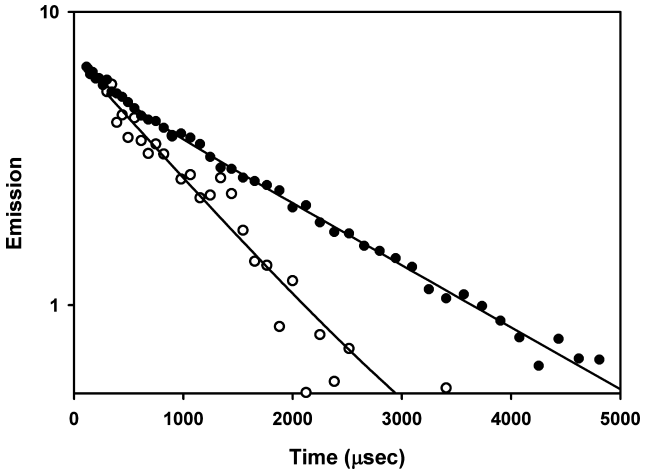

Figure 6. LRET between LBT and FlMTX. Tb−DAL complex (1.1 μM) lifetime in the absence of FlMTX (●) measured at 545 nm. The line was fit with a 2.05 ms lifetime. Tb−DAL complex lifetime after addition of 1.2 μM FlMTX (○), measured at 520 nm as sensitized emission from fluorescein, with a lifetime of 1.04 ms. The excitation wavelength was 280 nm.

yield (Figure 5) as 0.56, and from the change in lifetime (Figure 6) as 0.50. These results give distances between Tb^{3+} and fluorescein of 43 and 45 Å, respectively (Table 1).

GFP LRET Acceptor. GAL, a test protein similar to DAL, was constructed by putting GFP^{S65T} at the N-terminus, ankyrin repeats in the middle, and a lanthanide-binding tag (LBT) with a hexa-His tag at the C-terminus. Addition of Tb^{3+} showed the expected LRET from the Tb^{3+} energy donor to the GFP fluorophore energy acceptor, with a transfer efficiency of 0.69 and a calculated distance of 43 Å between the donor and acceptor (Table 1). GAL is somewhat less useful than DAL, because it is not straightforward to measure Tb^{3+} emission in the absence of the GFP fluorophore. For the calculation shown in Table 1, we assumed the lifetime of the Tb^{3+}−LBT complex was 2.0 ms in the absence of the GFP fluorophore.

Binding of Tb^{3+} to DAL in Live *E. coli* Cells. Four hours after the induction of DAL, *E. coli* cells were mixed with 50 μM Tb^{3+}, and the emission spectrum was immediately scanned (Figure 7). A large Tb^{3+} emission signal was observed (curve a, Figure 7), indicating that Tb^{3+} freely entered the cell and combined with the LBT of DAL. Control cells not expressing DAL showed little Tb^{3+} emission when 50 μM Tb^{3+} was added (curve d, Figure 7). The DAL was clearly associated with the *E. coli* cells, as shown when the cells were centrifuged and the emission of the supernatant was measured (curve c, Figure 7). When the periplasm was extracted from the cells,[18] we found at least 88% of the Tb^{3+} emission was in the cytoplasm. By comparing the emission signal from cells expressing DAL with a purified sample of DAL at a known concentration in free solution, we estimate that the cells in Figure 7 contained approximately 300000 molecules of DAL per cell.

To measure the rate of Tb^{3+} influx, we monitored the intensity of the emission at 545 nm as a function of time (Figure 8A). Influx data were fitted with two exponentials (Table 2), with ~80% of the intensity change associated with

dx.doi.org/10.1021/bi200779u | *Biochemistry* 2011, 50, 6789−6796

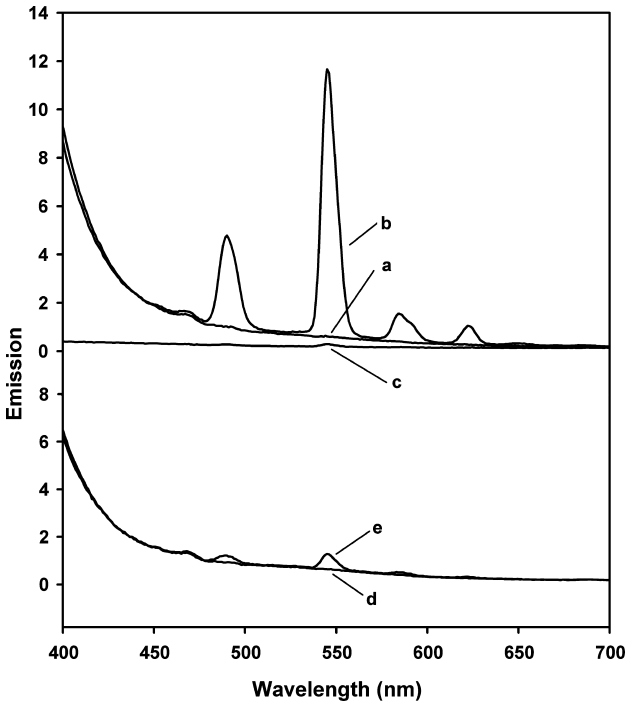

Figure 7. Uptake of terbium by live *E. coli* cells. Four hours after DAL induction, cells were suspended in buffer at a density of 0.3 mg of dry weight/mL (a). After addition of 50 μM Tb^{3+}, strong terbium luminescence is observed (b). Essentially no luminescence is in the supernatant after centrifugation (c). Control cells not expressing DAL (d) show little luminescence after addition of 50 μM Tb^{3+} (e). The excitation wavelength was 280 nm.

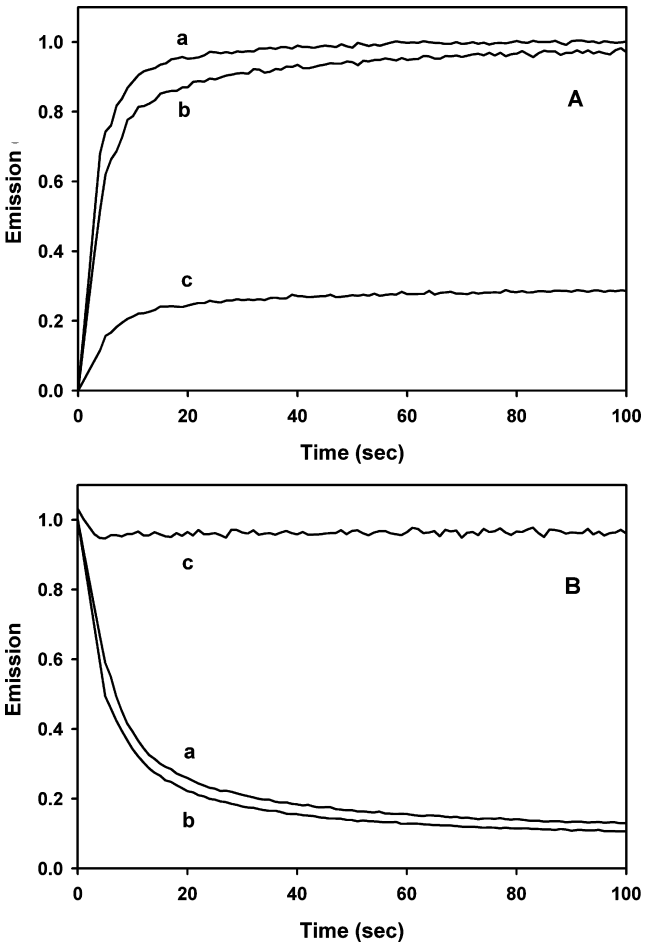

Figure 8. Kinetics of uptake of metal by live *E. coli* cells. (A) Terbium uptake, measured by formation of the DAL−Tb^{3+} complex: (a) 50 μM Tb^{3+} added to EDTA-washed cells (pH 7.0), (b) without EDTA treatment (pH 7.0), and (c) without EDTA treatment (pH 5.0). (B) Copper uptake, measured by LRET from the Tb^{3+}−DAL complex to the Cu^{2+}−DAL complex: (a) 10 μM Cu^{2+} added to cells without EDTA treatment, (b) 10 μM Cu^{2+} added to cells after EDTA pretreatment, and (c) 10 μM Cu^{+} added to cells without EDTA treatment. Excitation at 280 nm and emission at 545 nm.

the faster kinetic process. Uptake of Tb^{3+} was somewhat faster in cells that had been pretreated with EDTA, although not significant at the $p < 0.05$ level. Tb^{3+} uptake was not affected by CCCP, DCCD, or Ca^{2+} (Table 2), nor was uptake affected by pretreatment with glucose. A slight inhibitory effect was observed when the membrane potential was reversed by valinomycin-K^+ (Table 2). The extent of Tb^{3+} uptake decreased by three-quarters (Figure 8A) in cells suspended in pH 5.0 buffer, compared with cells in pH 7.0 buffer, and the rate of uptake was also slower (Table 2). When Cu^{2+} was added to cells that had been loaded with Tb^{3+}, the luminescence rapidly decreased (Figure 8B) to a level similar to that observed with the purified DAL−Tb^{3+} complex to which Cu^{2+} had been added (Table 1). This suggests that the DAL−Tb^{3+} complex is an indicator for transport of Cu^{2+} into *E. coli* cells. The uptake rates were fitted with two exponentials, the faster of which accounted for ∼60−80% of the intensity change (Table 2). Addition of Cu(I) (Cu^{2+} and dithiothreitol) had no effect on the Tb^{3+} luminescence (Figure 8B), as expected, because Cu(I) absorbance does not overlap Tb^{3+} emission, and therefore, it is not an LRET acceptor. Cu^{2+} influx rates were faster in cells pretreated with EDTA (Table 2). In the case of the slower kinetic process, the difference was significant at the $p < 0.05$ level. There was essentially no effect of CCCP, DCCD, or Ca^{2+} on Cu^{2+} influx (Table 2), and pretreatment with glucose had no effect. Reversal of the membrane potential with valinomycin-K^+ decreased the Cu^{2+} influx rate constant by a factor of ∼3 (Table 2). The Cu^{2+} uptake rate was slower in cells suspended in pH 5.0 buffer compared with cells in pH 7.0 buffer, and the kinetics were fit by only a single exponential, with the slower kinetic process not observed (Table 2).

DISCUSSION

DAL Structure. DAL is potentially useful as a test protein for LRET experiments. For example, in setting up an LRET microscope,[5] it is valuable to have a calibration standard. Common non-protein coordination compounds such as terbium dipicolinate can calibrate the intensity of direct terbium emission, but they lack an energy acceptor for testing LRET (except by diffusion transfer,[20] which requires relatively high donor and acceptor concentrations compared with the concentrations of labeled proteins that would typically be expressed in oocytes). With purified DAL, we measured LRET from Tb^{3+} to transition metals bound to the hexa-His tag and to fluorescein bound to the DHFR active site (Table 1). The distances are consistent with models built from the known crystal structures of the component domains. We used RosettaDock to obtain a probable interaction between the DHFR and ankyrin domains, and we used Autodock to identify

dx.doi.org/10.1021/bi200779u | *Biochemistry* 2011, 50, 6789−6796

Table 2. Uptake of Metal Ions by *E. coli* Cells

conditions[a]	first addition(s)[a]	k_1[b] (s^{-1})	k_2[b] (s^{-1})	A_1[b]	second addition[a]	k_1 (s^{-1})	k_2 (s^{-1})	A_1
pH 7, Na^+	Tb^{3+}	0.28 ± 0.05[c]	0.032 ± 0.015	0.82 ± 0.11	Cu	0.10 ± 0.03	0.016 ± 0.004[d]	0.65 ± 0.11
EDTA, pH 7, Na^+	Tb^{3+}	0.40 ± 0.15	0.048 ± 0.016	0.84 ± 0.04	Cu	0.18 ± 0.01	0.033 ± 0.002[d]	0.81 ± 0.01
pH 7, Na^+	CCCP, Tb^{3+}	0.29	0.032	0.85	Cu	0.092	0.016	0.62
EDTA, pH 7, K^+	val, Tb^{3+}	0.29	0.053	0.80	Cu	0.063	0.009	0.72
EDTA, pH 7, Na^+	val, Tb^{3+}	0.42	0.11	0.72	Cu	0.10	0.018	0.72
EDTA, pH 7, Na^+	DCCD, Tb^{3+}	0.51	0.043	0.86	Cu	0.17	0.03	0.77
pH 7, Na^+	Ca^{2+}, Tb^{3+}	0.24	0.022	0.83	Cu	0.077	0.013	0.6
EDTA, pH 7, Na^+	Ca^{2+}, Tb^{3+}	0.39	0.049	0.87	Cu	0.17	0.026	0.82
EDTA, pH 5, Na^+	Tb^{3+}	0.23	0.014	0.78	Cu	0.12	–	1

[a]See Materials and Methods and Results for details. [b]Rates of metal transport fitted with two exponentials: $L(t)/L_o = A_1 \exp(-k_1 t) + A_2 \exp(-k_2 t)$, where $L(t)$ is the luminescence measured at time t and L_o is $L(t)$ at time zero. [c]Plus or minus the standard deviation. [d]Significant at the $p < 0.05$ level.

the likely position of fluorescein in the DHFR active site. The fluorescein location predicted by Autodock is consistent with published chemical cross-linking data.[21] Depending on the orientation of the LBT domain, the modeled Tb^{3+}–fluorescein distance could be between 43 and 53 Å. The measured donor–acceptor distance (Table 1) was 43–45 Å. This measurement also confirms the conclusions of Zhang and Peng,[10] based on NMR, that the two C-terminal ankyrin domains of $p16^{INK4a}$ are sufficient for folding into a compact structure. Therefore, these two ankyrin domains could be generally useful as spacers in protein design.

Metal Transport. We found that living *E. coli* cells expressing DAL, a terbium-binding protein, displayed strong protein-sensitized Tb^{3+} emission when suspended in micromolar concentrations of $TbCl_3$. We showed that the Tb^{3+}–DAL complex was not in the extracellular medium, and most was in the cytoplasm when the periplasm was removed. Previous studies of the interaction of *E. coli* with terbium indicated an accumulation in the membranes and periplasm.[22] A recent study showed that *E. coli* cells were viable after being suspended at millimolar Tb^{3+} concentrations,[23] and a substantial amount of terbium was found inside the cell, although the distribution between the cytoplasm and periplasm was not determined. Thus, we have shown here for the first time Tb^{3+}, at concentrations that are not toxic, is imported into the cytoplasm by *E. coli*. This may be useful for future studies of metal transport and molecular structure.

The Tb^{3+}–DAL complex can be used as an indicator of the concentration of metals transported into the cytoplasm of *E. coli* in two different ways. Terbium can act as a calcium analogue,[24] so the increase in the magnitude of the Tb^{3+}–DAL signal may monitor calcium influx pathways. After the Tb^{3+}–DAL complex forms, binding of transition metals to the hexa-His tag site will quench Tb luminescence if their absorbance spectra overlap the Tb emission spectrum.[5] We used DAL to monitor the rates of Tb^{3+} and Cu^{2+} transport (Figure 8 and Table 2). Monitoring the uptake of Tb^{3+} via DAL is similar to previous studies using heterologously expressed aequorin to monitor rates of Ca^{2+} transport.[25] The Tb emission signal is related to the free cytoplasmic metal concentration as follows. The Tb^{3+} concentration in the cytoplasm ($[T_c]$) will change over time according to eq 1:

$$d[T_c]/dt = k_i[T_o] + k_d[T_D] - k_e[T_c] - k_a[T_c] \quad (1)$$

where k_i, k_d, k_e, and k_a are the rate constants for terbium influx, dissociation from DAL, efflux, and association with DAL, respectively, and $[T_o]$ and $[T_D]$ are the terbium concentrations outside the cell and the concentration of terbium bound to DAL, respectively. The dissociation constant K for dissociation of Tb^{3+} from DAL is given by

$$K = ([T_c][D])/[T_D] \quad (2)$$

where $[D]$ is the concentration of DAL without Tb^{3+} bound. When $[T_c] \gg K$

$$d[T_c]/dt = k_i[T_T] + (k_d - k_i)[D_T] - (k_e + k_a + k_i)[T_c] \quad (3)$$

where $[T_T]$ is the total Tb^{3+} concentration and $[D_T]$ is the total DAL concentration. Solving eq 3 with the boundary condition that $[T_c] = 0$ at time zero gives

$$[T_c] = (a/b)[1 - \exp(-bt)] \quad (4)$$

where $a = k_i[T_T] + (k_d - k_i)[D_T]$ and $b = k_e + k_a + k_i$. The luminescence signal, measured as Tb^{3+} combines with DAL upon entering the cell, arises from the increase in $[T_D]$, the time dependence of which can be obtained by combining eqs 3 and 4:

$$[T_D] = \frac{[D_T](a/b)[1 - \exp(-bt)]}{K + (a/b)[1 - \exp(-bt)]} \quad (5)$$

According to eq 5, the time dependence of the Tb^{3+}–DAL complex emission is related to the rate constants for both influx and efflux of terbium. A similar dependence on both influx and efflux rates would be expected for copper transport. Although the mathematical form is complicated, it can be shown numerically that equations of this form are well-fitted by a sum of two exponentials, which is what we observed for both the rates of terbium and copper transport (Table 2).

Calcium influx and efflux mechanisms have been previously identified in *E. coli*.[26,27] Some of these transporters depend on either a proton gradient or cytoplasmic ATP for activity. Thus, we tested the effect of proton and charge uncouplers and an ATP synthase inhibitor. The results indicated that the transport was insensitive to CCCP, valinomycin, and DCCD (Table 2). Furthermore, excess Ca^{2+} had no effect on terbium transport (Table 2). These results indicate that previously studied calcium transporters such as the Ca^{2+}/H^+ antiporter[28] and polyhydroxybutyrate channels[29] are not likely to be involved in the terbium uptake mechanism. Measured influx rates increase slightly after removal of lipopolysaccharide (EDTA treatment). The increase may be due to EDTA treatment providing higher periplasmic access and less competition from periplasmic

dx.doi.org/10.1021/bi200779u | *Biochemistry* 2011, 50, 6789–6796

binding sites. Membrane potential has a small influence on influx rates, as expected, because the uptake of terbium and copper is thermodynamically downhill. Although a low external pH had a dramatic inhibitory effect on the Tb^{3+}–DAL signal, this likely is due to a rapid equilibration of the cytoplasm with the external pH,[30,31] causing an inhibition of binding of terbium to DAL by protonation of the carboxyl ligands in the LBT binding site. This suggests the possibility that DAL can be used as a detector for cytoplasmic pH changes in the pH 5–6 range. Several mechanosensitive channels (Msc) have been studied in *E. coli* and are known to transport a variety of cations.[32,33] However, these are not likely to be involved in terbium transport, because the transport of cations through Msc is inhibited by lanthanides,[34] as is transport through polyhydroxybutyrate channels.[35] Future studies of copper transport using DAL may be helpful in characterizing transporters involved in Cu(II) influx in *E. coli*, which have not yet been identified.[36]

Whole Cell Structural Studies. We have shown that LRET can be measured in live *E. coli* cells at concentrations of terbium that are not toxic to the cells. Using genetically encoded tags, LBT as an LRET donor, and either hexa-His tags[5] or tetra-Cys sequences[37,38] for LRET acceptors could permit proximity measurements over shorter distances and with lower likelihood of structural disruption than with fluorescent proteins such as GFP. For cells the size of *E. coli*, these measurements would probably be restricted to studying slowly diffusing proteins, because a freely diffusing protein can travel distances in the range of cellular dimensions within the lifetime of the terbium excited state.[20,39] However, there are several interesting structural problems that could be addressed, including protein complexes,[40,41] bacterial microcompartments,[42] bacterial filaments,[43] and membrane assemblies.[44] Finally, LBT-directed terbium binding may be useful as a contrast agent in cryoelectron microscopy for molecular structure studies at the whole cell level.[45]

AUTHOR INFORMATION

Corresponding Author

*Department of Biology, University of Texas at San Antonio, San Antonio, TX 78249. E-mail: robert.renthal@utsa.edu. Phone: (210) 458-5452. Fax: (210) 458-4467.

Funding

This work was supported by National Institutes Health Grants R21DC010071 and G12RR013646 and San Antonio Life Sciences Institute Grant CB 3661.

ABBREVIATIONS

CCCP, [(3-chlorophenyl)hydrazono]malononitrile; DAL, engineered protein comprising (in order from the N-terminus) *E. coli* dihydrofolate reductase, ankyrin repeats 3 and 4 from $p16^{INK4a}$, a lanthanide-binding tag, and a hexa-His tag; DCCD, *N*,*N*′-dicyclohexylcarbodiimide; DHFR, dihyrofolate reductase; EDTA, 2,2′,2″,2‴-(ethane-1,2-diyldinitrilo)tetraacetic acid; FlMTX, fluorescein methotrexate; FRET, Förster resonance energy transfer; GAL, engineered protein similar to DAL except with GFP^{S65T} as the N-terminal domain; GFP, green fluorescent protein; HEPES, 2-[4-(2-hydroxyethyl)piperazin-1-yl]ethanesulfonic acid; LBT, lanthanide-binding tag; LRET, luminescence resonance energy transfer; PDB, Protein Data Bank.

REFERENCES

(1) Selvin, P. R. (2002) Principles and biophysical applications of lanthanide-based probes. *Annu. Rev. Biophys. Biomol. Struct. 31*, 275–302.

(2) Franz, K. J., Nitz, M., and Imperiali, B. (2003) Lanthanide-binding tags as versatile protein coexpression probes. *ChemBioChem 4*, 265–271.

(3) Nitz, M., Franz, K. J., Maglathlin, R. L., and Imperiali, B. (2003) A powerful combinatorial screen to identify high-affinity terbium(III)-binding peptides. *ChemBioChem 4*, 272–276.

(4) Sculimbrene, B. R., and Imperiali, B. (2006) Lanthanide-binding tags as luminescent probes for studying protein interactions. *J. Am. Chem. Soc. 128*, 7346–7352.

(5) Sandtner, W., Bezanilla, F., and Correa, A. M. (2007) In vivo measurement of intramolecular distances using genetically encoded reporters. *Biophys. J. 93*, L45–L47.

(6) Rajapakse, H. E., Reddy, D. R., Mohandessi, S., Butlin, N. G., and Miller, L. W. (2009) Luminescent terbium protein labels for time-resolved microscopy and screening. *Angew. Chem., Int. Ed. 48*, 4990–4992.

(7) Montgomery, C. P., Murray, B. S., New, E. J., Pal, R., and Parker, D. (2009) Cell-penetrating metal complex optical probes: Targeted and responsive systems based on lanthanide luminescence. *Acc. Chem. Res. 42*, 925–937.

(8) Deiters, E., Song, B., Chauvin, A. S., Vandevyver, C. D., Gumy, F., and Bunzli, J. C. (2009) Luminescent bimetallic lanthanide bioprobes for cellular imaging with excitation in the visible-light range. *Chemistry 15*, 885–900.

(9) Rajapakse, H. E., Gahlaut, N., Mohandessi, S., Yu, D., Turner, J. R., and Miller, L. W. (2010) Time-resolved luminescence resonance energy transfer imaging of protein-protein interactions in living cells. *Proc. Natl. Acad. Sci. U.S.A. 107*, 13582–13587.

(10) Zhang, B., and Peng, Z. (2000) A minimum folding unit in the ankyrin repeat protein p16(INK4). *J. Mol. Biol. 299*, 1121–1132.

(11) Stemmer, W. P., Crameri, A., Ha, K. D., Brennan, T. M., and Heyneker, H. L. (1995) Single-step assembly of a gene and entire plasmid from large numbers of oligodeoxyribonucleotides. *Gene 164*, 49–53.

(12) Crameri, A., Whitehorn, E. A., Tate, E., and Stemmer, W. P. (1996) Improved green fluorescent protein by molecular evolution using DNA shuffling. *Nat. Biotechnol. 14*, 315–319.

(13) Touchette, N. A., Perry, K. M., and Matthews, C. R. (1986) Folding of dihydrofolate reductase from *Escherichia coli*. *Biochemistry 25*, 5445–5452.

(14) Humphrey, W., Dalke, A., and Schulten, K. (1996) VMD: Visual molecular dynamics. *J. Mol. Graphics 14*, 27–38.

(15) Morris, G. M., Huey, R., Lindstrom, W., Sanner, M. F., Belew, R. K., Goodsell, D. S., and Olson, A. J. (2009) AutoDock4 and AutoDockTools4: Automated docking with selective receptor flexibility. *J. Comput. Chem. 30*, 2785–2791.

(16) Koch, A. L. (1970) Turbidity measurements of bacterial cultures in some available commercial instruments. *Anal. Biochem. 38*, 252–259.

(17) Joshi, A. K., Ahmed, S., and Ferro-Luzzi Ames, G. (1989) Energy coupling in bacterial periplasmic transport systems. Studies in intact *Escherichia coli* cells. *J. Biol. Chem. 264*, 2126–2133.

(18) Nossal, N. G., and Heppel, L. A. (1966) The release of enzymes by osmotic shock from *Escherichia coli* in exponential phase. *J. Biol. Chem. 241*, 3055–3062.

(19) Rosowsky, A., Wright, J. E., Shapiro, H., Beardsley, P., and Lazarus, H. (1982) A new fluorescent dihydrofolate reductase probe for studies of methotrexate resistance. *J. Biol. Chem. 257*, 14162–14167.

(20) Stryer, L., Thomas, D. D., and Meares, C. F. (1982) Diffusion-enhanced fluorescence energy transfer. *Annu. Rev. Biophys. Bioeng. 11*, 203−222.

(21) Gallagher, S. S., Sable, J. E., Sheetz, M. P., and Cornish, V. W. (2009) An in vivo covalent TMP-tag based on proximity-induced reactivity. *ACS Chem. Biol. 4*, 547−556.

(22) Bayer, M. E., and Bayer, M. H. (1991) Lanthanide accumulation in the periplasmic space of *Escherichia coli* B. *J. Bacteriol. 173*, 141−149.

(23) Achyuthan, K. E., Arango, D. C., Carles, E. L., Cutler, C. E., Meyer, L. A., and Brozik, S. M. (2009) Luminescent investigations of terbium(III) biosorption as a surrogate for heavy metals and radionuclides. *Mol. Cell. Biochem. 327*, 87−92.

(24) Martin, R. B., and Richardson, F. S. (1979) Lanthanides as probes for calcium in biological systems. *Q. Rev. Biophys. 12*, 181−209.

(25) Jones, H. E., Holland, I. B., Baker, H. L., and Campbell, A. K. (1999) Slow changes in cytosolic free Ca^{2+} in *Escherichia coli* highlight two putative influx mechanisms in response to changes in extracellular calcium. *Cell Calcium 25*, 265−274.

(26) Holland, I. B., Jones, H. E., Campbell, A. K., and Jacq, A. (1999) An assessment of the role of intracellular free Ca^{2+} in *E. coli*. *Biochimie 81*, 901−907.

(27) Naseem, R., Wann, K. T., Holland, I. B., and Campbell, A. K. (2009) ATP regulates calcium efflux and growth in *E. coli*. *J. Mol. Biol. 391*, 42−56.

(28) Ivey, D. M., Guffanti, A. A., Zemsky, J., Pinner, E., Karpel, R., Padan, E., Schuldiner, S., and Krulwich, T. A. (1993) Cloning and characterization of a putative Ca^{2+}/H^{+} antiporter gene from *Escherichia coli* upon functional complementation of Na^{+}/H^{+} antiporter-deficient strains by the overexpressed gene. *J. Biol. Chem. 268*, 11296−11303.

(29) Reusch, R. N., and Sadoff, H. L. (1988) Putative structure and functions of a poly-*β*-hydroxybutyrate/calcium polyphosphate channel in bacterial plasma membranes. *Proc. Natl. Acad. Sci. U.S.A. 85*, 4176−4180.

(30) Naseem, R., Holland, I. B., Jacq, A., Wann, K. T., and Campbell, A. K. (2008) pH and monovalent cations regulate cytosolic free Ca^{2+} in *E. coli*. *Biochim. Biophys. Acta 1778*, 1415−1422.

(31) Kitko, R. D., Wilks, J. C., Garduque, G. M., and Slonczewski, J. L. (2010) Osmolytes contribute to pH homeostasis of *Escherichia coli*. *PLoS One 5*, e10078.

(32) Corry, B., and Martinac, B. (2008) Bacterial mechanosensitive channels: Experiment and theory. *Biochim. Biophys. Acta 1778*, 1859−1870.

(33) Anishkin, A., and Sukharev, S. (2009) State-stabilizing Interactions in Bacterial Mechanosensitive Channel Gating and Adaptation. *J. Biol. Chem. 284*, 19153−19157.

(34) Ermakov, Y. A., Kamaraju, K., Sengupta, K., and Sukharev, S. (2010) Gadolinium ions block mechanosensitive channels by altering the packing and lateral pressure of anionic lipids. *Biophys. J. 98*, 1018−1027.

(35) Campbell, A. K., Naseem, R., Wann, K., Holland, I. B., and Matthews, S. B. (2007) Fermentation product butane 2,3-diol induces Ca^{2+} transients in *E. coli* through activation of lanthanum-sensitive Ca^{2+} channels. *Cell Calcium 41*, 97−106.

(36) Osman, D., and Cavet, J. S. (2008) Copper homeostasis in bacteria. *Adv. Appl. Microbiol. 65*, 217−247.

(37) Adams, S. R., and Tsien, R. Y. (2008) Preparation of the membrane-permeant biarsenicals FlAsH-EDT2 and ReAsH-EDT2 for fluorescent labeling of tetracysteine-tagged proteins. *Nat. Protoc. 3*, 1527−1534.

(38) Romantsov, T., Battle, A. R., Hendel, J. L., Martinac, B., and Wood, J. M. (2010) Protein localization in *Escherichia coli* cells: Comparison of the cytoplasmic membrane proteins ProP, LacY, ProW, AqpZ, MscS, and MscL. *J. Bacteriol. 192*, 912−924.

(39) Nenninger, A., Mastroianni, G., and Mullineaux, C. W. (2010) Size dependence of protein diffusion in the cytoplasm of *Escherichia coli*. *J. Bacteriol. 192*, 4535−4540.

(40) Rudner, D. Z., and Losick, R. (2010) Protein subcellular localization in bacteria. *Cold Spring Harbor Perspect. Biol. 2*, a000307.

(41) Vendeville, A., Lariviere, D., and Fourmentin, E. (2011) An inventory of the bacterial macromolecular components and their spatial organization. *FEMS Microbiol. Rev. 35*, 395−414.

(42) Yeates, T. O., Crowley, C. S., and Tanaka, S. (2010) Bacterial microcompartment organelles: Protein shell structure and evolution. *Annu. Rev. Biophys. 39*, 185−205.

(43) Salje, J., Zuber, B., and Lowe, J. (2009) Electron cryomicroscopy of *E. coli* reveals filament bundles involved in plasmid DNA segregation. *Science 323*, 509−512.

(44) Kentner, D., and Sourjik, V. (2006) Spatial organization of the bacterial chemotaxis system. *Curr. Opin. Microbiol. 9*, 619−624.

(45) Milne, J. L., and Subramaniam, S. (2009) Cryo-electron tomography of bacteria: Progress, challenges and future prospects. *Nat. Rev. Microbiol. 7*, 666−675.